Analysis of a SD-OCT-based hyperspectral system for spectral reflectance measurements

Maria, Michael; Anisimov, Andrei G.; Stols-Witlox, Maartje; Groves, Roger M.

DOI
10.1117/12.2555435

Publication date
2020

Document Version
Final published version

Published in
Optical Sensing and Detection VI

Analysis of a SD-OCT-based hyperspectral system for spectral reflectance measurements

Maria, Michael, Anisimov, Andrei, Stols-Witlox, Maartje, Groves, Roger

Michael Maria, Andrei G. Anisimov, Maartje Stols-Witlox, Roger M. Groves, "Analysis of a SD-OCT-based hyperspectral system for spectral reflectance measurements," Proc. SPIE 11354, Optical Sensing and Detection VI, 113541J (1 April 2020); doi: 10.1117/12.2555435

SPIE.

Event: SPIE Photonics Europe, 2020, Online Only

Analysis of a SD-OCT-based hyperspectral system for spectral reflectance measurements

Michael Maria*[a], Andrei G. Anisimov[a], Maartje Stols-Witlox[b] and Roger M. Groves[a]
[a]Structural Integrity and Composites, Faculty of Aerospace Engineering, Delft University of Technology, Kluyverweg 1, 2629 HS Delft, The Netherlands
[b]Conservation & Restoration, University of Amsterdam, Johannes Vermeerplein 1, 1071 DV Amsterdam, The Netherlands

ABSTRACT

In this study, we compare the hyperspectral imaging capabilities of a custom-built visible light OCT with those of a commercial grade hyperspectral camera. Using the Short-Time-Fourier-Transform algorithm on the OCT signal, we estimate the variation in the surface spectral response from two paint pigments. Our study aims at comparing the spectral measurements obtained from calibration samples and to estimate an optimal working point for OCT-based hyperspectral processing.
Keywords: Optical Coherence Tomography, Hyperspectral Imaging, Spectroscopy, Spectral Calibration

1. INTRODUCTION

Optical Coherence Tomography is an imaging modality which provides structural information about semi-transparent samples [1]. Since the introduction of OCT in 1991, many extensions of the technique have been developed, among others OCT-Angiography (OCTA), Spectroscopic-OCT, (sOCT) and Optical Coherence Elastography (OCE), which provide additional contrast compared to conventional OCT. Those complementary contrasts can be used to identify other particular conditions of the sample, for example flow [2], stiffness [3] or spectral properties [4]. Within such extensions, sOCT has been applied mostly to measure oxygenation within blood vessels in order to investigate topics such as the mechanism behind a stroke [5] or the effects of the Alzheimer disease on brain tissue [6].

Spectroscopic-OCT takes advantage of the broad optical bandwidth required for high axial resolution in OCT, to extract localized spectral knowledge within the sample of interest. Several techniques are available for extracting spectral information from an OCT dataset. The most popular are Short-Time-Fourier-Transform (STFT), Wavelet-Transform (WT), Dual-Window (DW) and the Wigner-Ville-Distribution (WVD) [4]. Although different in the processing details, all these approaches share the philosophy of using processing of the sub-bands within the optically broad OCT signal to obtain a spectrally resolved representation of the sample. A well-known trade-off of sOCT analysis is by the inverse relation between spectral and spatial resolution. High spatial resolution requires large optical bandwidth and leads to low spectral resolution. Vice-versa, high spectral resolution leads to poor spatial resolution. Progress has been made. Since the early demonstration of sOCT, Supercontinuum (SC) light sources have improved and have been proven to be highly effective at driving OCT systems in the Near Infrared (NIR) and in the visible (Vis) regions [5,7,8] with optical bandwidth easily exceeding the spectral detection range of common spectrometers. Nowadays, sOCT is nearly always based on the association of a SC light source and an Ultra-High Resolution-OCT (UHR-OCT) system. State of the art sOCT can reach spectral resolutions in the 10 nm range with a spatial resolutions below 10 µm [6,9].

While mostly used in the context of biomedical application, OCT is also a highly relevant tool for Non-Destructive Investigation (NDI) in other fields, as shown by applications in fields ranging from industrial coating inspection [10] to art research and cultural heritage conservation [11]. In cultural heritage research, NIR light OCT is most common, as longer wavelengths lead to lower scattering, resulting in increased depth penetration, of importance for this particular application. Liang & al showed that for this conventional approach, the optimal wavelength range is around 2 µm [11]. Using long-wavelength OCT, several studies have demonstrated the existence of underdrawings or the presence of hidden characters or objects on old master paintings [12]. As successful as these studies have been, their focus was limited to revealing hidden/invisible portions of paintings, while this is only a part of the work conducted by art and conservation scientists. Indeed, reaching a better understanding of the visible portion of paintings is crucial for a better understanding of the work of a painter. Such information not only has relevance for research into conservation processes, but it has a high

Optical Sensing and Detection VI, edited by Francis Berghmans, Anna G. Mignani, Proc. of SPIE
Vol. 11354, 113541J · © 2020 SPIE · CCC code: 0277-786X/20/$21 · doi: 10.1117/12.2555435

value for the interpretation of paintings. In this study, we propose to use Vis-OCT to probe with ultra-high resolution the paint layers that influence the perception of the painting by the observer, which are the more thinly applied paint layers. In addition, by using algorithms similar to those used in the biomedical field (STFT), we investigate the possibility of identifying paint colors using the OCT readouts. This work is connected to the Down To The Ground project [13], in which the results of the OCT inspection will be used directly by a consortium of technical art historians and conservators.

2. OPTICAL INSTRUMENTS

2.1 Visible Optical Coherence Tomography system

The Vis-OCT system used in this study is based on 4 main components. First, the light source is a Supercontinuum (Electro VISIR- Leukos (France)). Its full spectrum spans from 450 nm to 2400 nm, and has a total optical power of around 200 mW. The OCT bandwidth (400 nm – 700 nm) is filtered using bulk optical filters and offers an optical power around 8 mW. Second, the interferometer is based on bulk optics, as sketched in Fig. 1, in order to operate with minimal chromatic effects. Third, light is detected using an ultra-broad spectrometer (COBRA VIS – Wasatch Photonics (United States)), which has a sensitivity bandwidth that spans from 500 nm to 700 nm. Fourth, the last part of the system is the custom-designed interface, consisting of many components (Galvo-scanner, Digital-to-Analog converter, etc.) through LabVIEW software for data acquisition. Post-processing of data is conducted using dedicated Matlab programs.

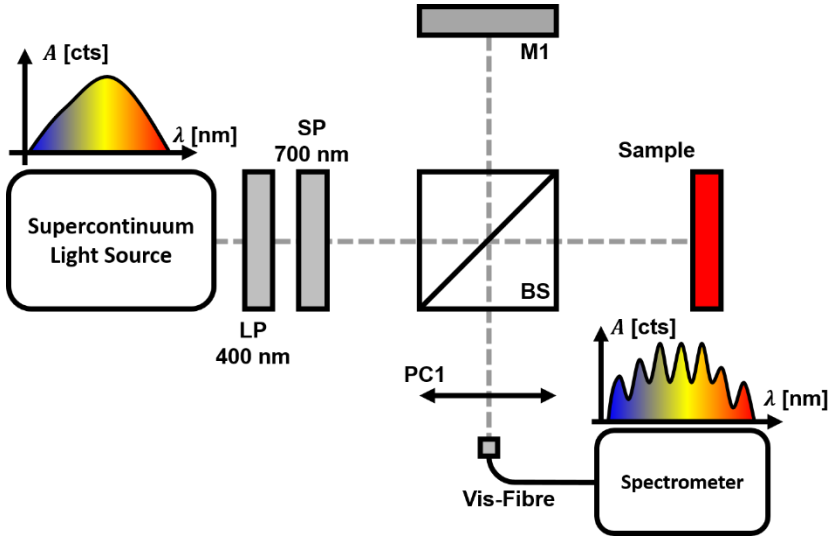

Figure 1: Schematic representation of the Vis-OCT system. LP: Long Pass filter, SP: Short Pass filter, BS: Beam Splitter, M1: Flat Mirror, PC1: Parabolic Collimator, Vis-Fiber: Optical Fiber for visible light.

2.2 Hyperspectral Camera

To provide a spectral reference the reflectance spectra are measured with a line-scan hyperspectral camera (IMSPECTOR V10E – Specim (Finland) with line pixel resolution of 1312 pixels, spectral range of 400-1000 nm, spectral resolution of 2.8 nm). A picture of the camera configuration is shown in Fig. 2. The spectra are averaged over an area of 40x50 mm, where 40 mm range is the line-field of view of the camera with a 35 mm lens and 50 mm range is the translation of the specimen during the measurements with the built-in scanning stage. An additional spectral flattening filter (Specim©) is used in front of the objective lens to improve the spectral uniformity. To avoid specular reflections, the light sources (3 tungsten 30W Halogen) are set at a 45-degree angle of incidence with respect to the sample and the camera.

Spectral and spatial calibration are performed for each camera pixel by recording dark (with camera shutter closed) and white reference fields (with a reference sample Spectralon SRT-M5-050 – Laser 2000). Subsequently, the recorded specimen spectra is normalized, to flatten the spectral curves and to compensate the non-uniform light distribution over the image field due to the varying illumination and the lens intensity distribution over the field of view. The calibration and the spectra processing are done using the Tensor Image Processing Platform (TIPP) developed by TU Delft and FORTH [14].

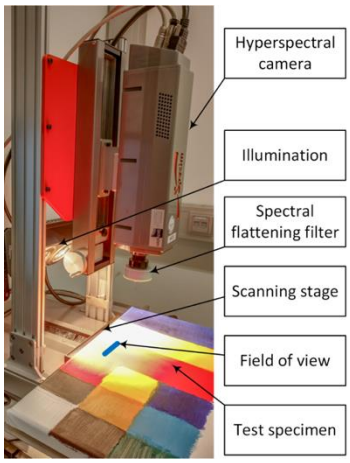

Figure 2: Hyperspectral camera configuration

3. SPECTROSCOPIC OCT SIGNAL PROCESSING

3.1 Spectroscopic Optical Coherence Tomography – Short Time Fourier Transform algorithm

Classical processing of data in Spectral Domain – OCT (SD-OCT) is based on Fourier analysis of the interference signal detected by the spectrometer. This interference signal, assuming the context of a Spectral Domain – OCT (SD-OCT) system, can be written as,

$$I(k) = I_R(k) + I_S(k) + 2\sqrt{I_R(k) I_S(k)} \times \cos(2kz). \quad (1)$$

with $I(k)$ as the total intensity detected by the spectrometer, $I_R(k)$ and $I_S(k)$ the intensities returning from the reference path and sample path respectively. k is the angular wavenumber and z is half of the length mismatch between reference path and the sample path of the interferometer. Then, the axial profile corresponding to $I(k)$, can be written as,

$$I(z) = \left| FT\left[I(k) \right] \right|^2 \quad (2)$$

with FT[] being the Fourier Transform operator.

For sOCT processing, a similar approach is used. However, instead of applying the FT operation to the entire optical bandwidth Δk, a series of sub-bands are considered instead. The STFT of $I(k)$ per sub-band is calculated as,

$$STFT_{I(k)}(z) = \left| FT\left[I(k) \times W(k', \Delta k') \right] \right|^2 \quad (3)$$

where W being an analysis windows centered at an angular wavenumber k' and spectral width $\Delta k'$.

The key point in using the STFT algorithm is in the difference between an axial profile obtained through either the conventional or the STFT approach. As the STFT axial profile is obtained by considering only a limited range of angular wavenumbers $\Delta k'$, the amplitude of the signal is a representation of the interaction between light and the sample of interest within this spectral region. Hence, it is a representation of the spectral properties of the sample at k'. Then, by varying the central angular wavenumber of the window W, it is possible to estimate the spectral response of the sample along the full bandwidth Δk.

4. PRELIMINARY RESULTS – MEASURING SURFACE SPECTRAL REFLECTANCE OF MONO-COLOR PAINT LAYER

4.1 Pre-processing of OCT readouts

Conventional OCT and sOCT both rely on a Fast Fourier Transform (FFT) operation to decompose the fringes signal in the Fourier domain. It is necessary, to have the signal described along equally-spaced wavenumber points prior to the FFT

operation. The common method used in this context is called data resampling and consists of an interpolation of the raw readouts along a pre-defined uniformly distributed wavenumber axis. In addition, the non-identical optical path length between the reference path and the sample path in the interferometer leads to dispersion effects in the OCT dataset. This means that it is important to compensate for dispersion prior to FFT operation, to ensure optimal signal-to-noise ratio and axial resolution in both OCT and sOCT. Fig. 3 shows the normalized Point Spread Functions (PSFs), processed similarly [15], obtained by using a mirror placed at a depth of 25 µm as an object. It is clear that some dispersion effects affect the OCT readouts as the dispersion compensated PSF is around half the width in terms of full-width-at-half-maximum of the resampling only PSF. In the next part of this paper, all OCT readouts will be fully pre-processed with resampling and dispersion compensation.

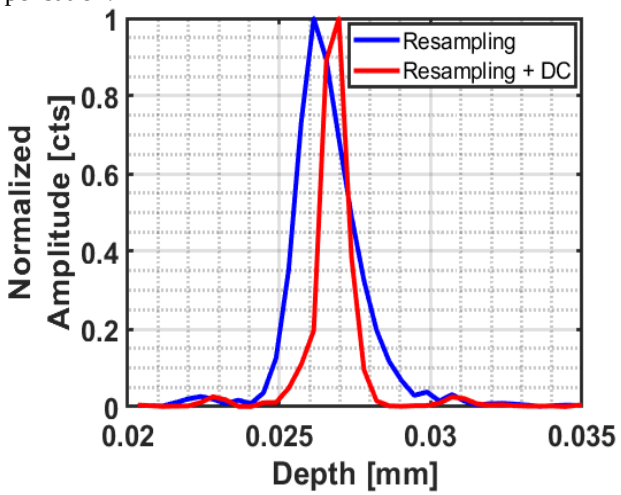

Figure 3: Axial point spread function measured using a mirror placed at a depth (in air) of 25 µm.

4.2 Imaging of mono-color layers of paint using Vis-OCT and the Hyperspectral Camera.

In order to estimate the possibilities to extract spectral measurements from the OCT data, two different paint layers (yellow and red) of the specimen in Fig. 2 are measured using the two imaging systems (Vis-OCT and Hyperspectral camera). The structural images obtained with the Vis-OCT system are shown in Fig. 4. As expected no particular differences can be seen in the pure structural information. For both images, the penetration depth is in the few tens of micrometer range, due to the large scattering of visible light. The axial resolution (estimated at the paint surface) matches those shown in Fig. 3.

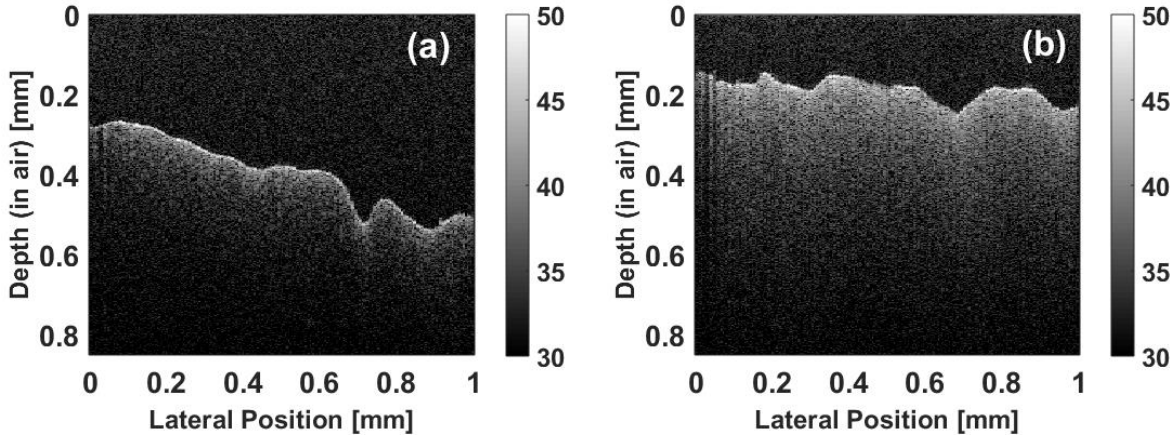

Figure 4: Structural images obtained using the Vis-OCT system. (a) Red paint and (b) Yellow paint regions.

Spectral information about the surface of the paint layers can be obtained from the OCT system via a direct reflectance approach. To do so, the reference path of the interferometer has to be blocked. Such a configuration corresponds simply to direct reflectance measurement similar to those obtained using the hyperspectral camera. Fig. 5 shows the surface

reflectance spectra obtained with the Vis-OCT and with the hyperspectral camera. In both cases the spectra show the reflectance expected of a yellow and red object and match the literature [16]. As the Vis-OCT-based measurements rely on a spectrometer for detecting reflected light, there is a sensitivity decrease at the edges of the spectral range due to geometrical aberrations within the spectrometer. This explains the signal drop at longer wavelengths (>640 nm) shown in Fig. 5(b). Another noticeable difference between the two types of reflectance spectra is the much larger error observed in the Vis-OCT based measurements. This difference can be attributed to more components complexity for the Vis-OCT (flying spot) compared to the hyperspectral camera (full-field).

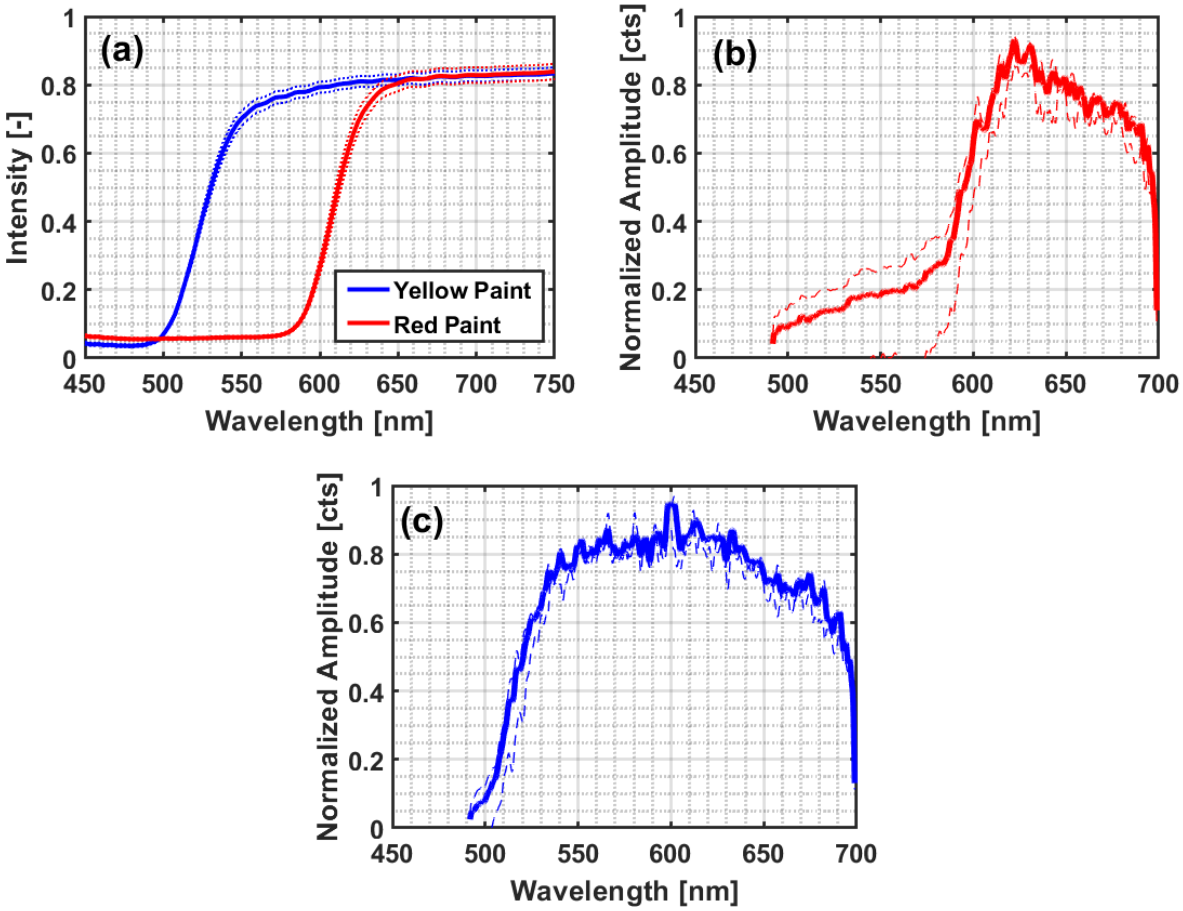

Figure 5: Direct reflectance measurements. (a) Hyperspectral Camera, (b) Vis-OCT based measurements for red pigment and Vis-OCT based measurements for yellow pigment. Average values (continuous lines), standard deviation (dotted lines).

Fig. 6 (a) and (b) show the respective normalized surface reflectance spectra measured with the Vis-OCT using the STFT algorithm for the red and yellow paint layer. Both reflectance curves are obtained by averaging a series of 250 spectra acquired from the specimen along a 1 mm line, followed up by a normalization step. Both paint layers can be relatively well identified from the measured reflectance. The red paint layer reflectance shows a relatively fast increase around a wavelength of 600 nm. That is similar to the direct reflectance measurements. However, a sharper transition is shown in the two other reflectance measurements. Considering the yellow paint layer, as expected the reflectance rise occurs at a wavelength around 500 nm, which is similar to the two other reflectance measurements. Also, the same seemingly slower rise of the reflectance values occurs. One significant feature which can be observed for the Vis-OCT reflectance measurements is the large deviation around the average values. Similar to the direct reflectance plot, an important deviation can be attributed to the flying spot configuration of the system, which then corresponds to varying backscattering signals into the interferometer for each transverse location. In order to obtain more accurate reflectance measurements using the Vis-OCT system, careful calibration and compensation needs to be applied prior to the STFT algorithm.

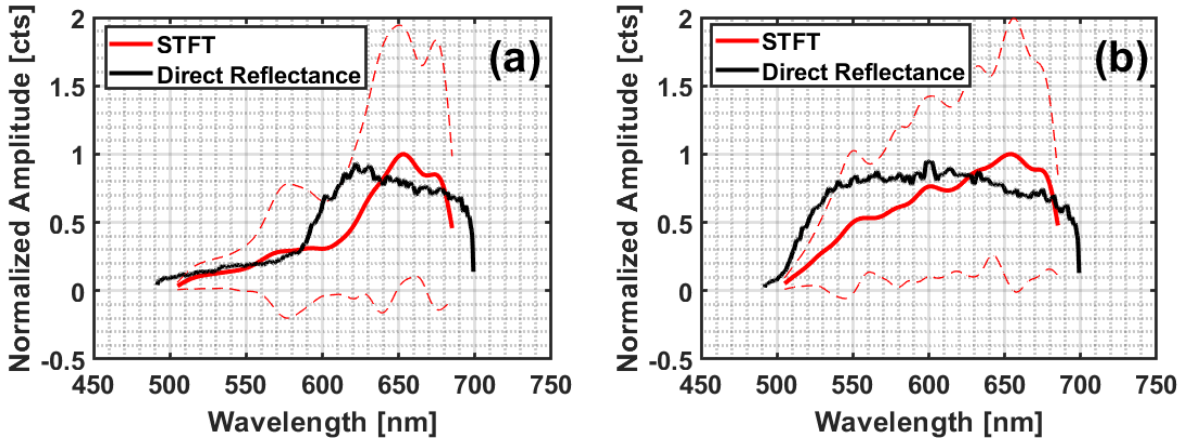

Figure 6: Measured spectral reflectance using the Vis-OCT system. (a) Red paint layer, (b) Yellow paint layer. Average values (continuous lines), standard deviation (dashed lines).

5. CONCLUSION

In this paper, we present the preliminary results from reconstructing spectral reflectance of an object using an OCT system. Using STFT algorithm on the OCT spectra, we measured the surface spectral reflectance of two differently colored paints and we compared them with the reflectance measured with a commercial grade hyperspectral camera. Initial results are promising, as our OCT-based curves match reasonably well with the hyperspectral based one in terms of overall shapes. However, the random errors in the spectral reflectance from the OCT-based spectra are still very high and further investigations will be carried out in order to implement corrections and compensations of signal fluctuation within the OCT system to reduce this error.

6. ACKNOWLEDGMENT

This work is supported by the Dutch Research Council (NWO) through the project *Down To The Ground*: *A Historical, Visual and Scientific Analysis of Coloured Grounds in Netherlandish Paintings, 1550-1650* (VC.GW17.029).

REFERENCES

[1] Huang, D., Swanson, E. A., Lin, C.P., Schuman, J. S., Stinson, W. G., Chang, W., Hee, M. R., Flotte, T., Gregory, K., Puliafito, C. A., Fujimoto, J. G., "Optical Coherence Tomography," Science 254(5035), 1178-1181 (1991).

[2] Chen, C. L. and Wang, R. K., "Optical coherence tomography based angiography," Biomed. Opt. Express 8, 1056-1082 (2017).

[3] Larin, K. V. and Sampson, D. D., "Optical coherence elastography – OCT at work in tissue biomechanics," Biomed. Opt. Express 8, 1172-1202 (2017).

[4] Bosschaart, B., van Leeuwen, T. G., Aalders, M. C. G, and Faber, D. J., "Quantitative comparison of analysis methods for spectroscopic optical coherence tomography," Biomed. Opt. Express 4, 2570-2584 (2013).

[5] Chen, S., Liu, Q., Shu, X., Soetikno, B., Tong, S. and Zhang, H. F. "Imaging hemodynamic response after ischemic stroke in mouse cortex using visible-light optical coherence tomography," Biomed. Opt. Express 7, 3377-3389 (2016).

[6] Lichtenegger, A., Harper, D. J., Augustin, M., Eugui, P., Muck, M., Gesperger, J., Hitzenberger, C. K., Woehrer, A., and Baumann, B., "Spectroscopic imaging with spectral domain visible light optical coherence microscopy in Alzheimer's disease brain samples," Biomed. Opt. Express 8, 4007-4025 (2017).

[7] Maria, M., Gonzalo, I. B., Bondu, M., Engelsholm, R. D., Feuchter, T., Moselund, P.M., Leick, L., Bang, O. and Podoleanu, A. "A comparative study of noise in supercontinuum light sources for ultra-high resolution optical coherence tomography", Proc. SPIE 10056, Design and Quality for Biomedical Technologies X, 100560O (14 March 2017); https://doi.org/10.1117/12.2251500

[8] Jensen, M., Gonzalo, I. B., Engelsholm, R. D., Maria, M., Israelsen, N. M., Podoleanu and A. Bang, O. "Noise of supercontinuum sources in spectral domain optical coherence tomography," J. Opt. Soc. Am. B 36, A154-A160 (2019).
[9] Harper, D. J., Konegger, T., Augustin, M., Schützenberger, K., Eugui, P., Lichtenegger, A., Merkle, C. W., Hitzenberger, C. K., Glösmann, M. and Baumann, B., "Hyperspectral optical coherence tomography for in vivo visualization of melanin in the retinal pigment epithelium," J. Biophotonics. 2019; 12:e201900153. https://doi.org/10.1002/jbio.201900153
[10] Czajkowski, J., Fabritius, T., Ulański, J., Marszałek, M., Gazicki-Lipman, M., Nosal, A., Śliż, R., Alarousu, E., Prykäri, T., Myllylä, R. and Jabbour, G. Ultra-high resolution optical coherence tomography for encapsulation quality inspection. *Appl. Phys. B* **105,** 649–657 (2011). https://doi.org/10.1007/s00340-011-4699-5
[11] Liang, H., Lange, R., Peric, B. and Spring, M. Optimum spectral window for imaging of art with optical coherence tomography. *Appl. Phys. B* **111,** 589–602 (2013). https://doi.org/10.1007/s00340-013-5378-5
[12] Targowski, P., Iwanicka, M. Optical Coherence Tomography: its role in the non-invasive structural examination and conservation of cultural heritage objects a review. *Appl. Phys. A* **106,** 265–277 (2012). https://doi.org/10.1007/s00339-011-6687-3
[13] Maartje Stols-Witlox, "Down To The Ground", University of Amsterdam, https://ahm.uva.nl/content/projects/down-to-the-ground/down-to-the-ground.html (05 March 2020).
[14] Papadakis, V., "The Tensor Image Processing Platform (TIPP)", FORTH, http://tipp.gr (25 February 2020).
[15] Bradu, A., Israelsen, N.M., Maria, M., Marques, M. J., Rivet, S., Feuchter, T., Bang, O. and Podoleanu, P. Recovering distance information in spectral domain interferometry. Sci Rep 8, 15445 (2018) doi:10.1038/s41598-018-33821-0
[16] Pottier, F., Gerardin, M., Michelin, A., Hébert, M., Andraud, C., "Simulating the composition and structuration of coloring layers in historical painting from non-invasive spectral reflectance measurements, " *Comptes Rendus Physique*, 19 (7), 599-611 (2018). https://doi.org/10.1016/j.crhy.2018.09.007.